

# ESTIMATING FIBRE DIRECTION DISTRIBUTIONS OF REINFORCED COMPOSITES FROM TOMOGRAPHIC IMAGES

OLIVER WIRJADI<sup>1</sup>, KATJA SCHLADITZ<sup>✉,1</sup>, PRAKASH EASWARAN<sup>1,2</sup> AND JOACHIM OHSER<sup>3</sup>

<sup>1</sup>Fraunhofer ITWM, Fraunhofer-Platz 1, D-67663 Kaiserslautern, Germany; <sup>2</sup>University of Kaiserslautern, Germany; <sup>3</sup>Hochschule Darmstadt, Fachbereich Mathematik und Naturwissenschaften, Schöfferstraße 3, D-64295 Darmstadt, Germany

e-mail: oliver.wirjadi@gmail.com, katja.schladitz@itwm.fraunhofer.de, prakash.easwaran@itwm.fraunhofer.de, joachim.ohser@h-da.de

(Received February 24, 2016; revised October 10, 2016; accepted November 2, 2016)

## ABSTRACT

Fibre reinforced composites constitute a relevant class of materials used chiefly in lightweight constructions for example in fuselages or car bodies. The spatial arrangement of the fibres and in particular their direction distribution have huge impact on macroscopic properties and, thus, its determination is an important topic of material characterisation. The fibre direction distribution is defined on the unit sphere, and it is therefore preferable to work with fully three-dimensional images of the microstructure as obtained, *e.g.*, by computed micro-tomography. A number of recent image analysis algorithms exploit local grey value variations to estimate a preferred direction in each fibre point. Averaging these local results leads estimates of the volume-weighted fibre direction distribution. We show how the thus derived fibre direction distribution is related to quantities commonly used in engineering applications. Furthermore, we discuss four algorithms for local orientation analysis, namely those based on the response of anisotropic Gaussian filters, moments and axes of inertia derived from directed distance transforms, the structure tensor, or the Hessian matrix. Finally, the feasibility of these algorithms is demonstrated for application examples and some advantages and disadvantages of the underlying methods are pointed out.

Keywords: composites, fibre direction distribution, image analysis, orientation tensor, tomography.

## INTRODUCTION

Light-weight construction in various contexts is one of the main driving forces behind the increasing application of fibre-reinforced materials. The microstructure of these materials is largely responsible for their favorable mechanical properties. Especially the directional distribution of the fibre system influences their tensile strength. This fact is also accounted for in modern tools for macroscopic material property simulation, leading to an increasing demand for precise measurement of local fibre volume content and fibre directions.

Early work has focused on the estimation of fibre direction distributions from planar sections through the material. Obviously, a planar cross-section of a straight cylinder is up to edge effects an ellipse whose aspect ratio depends on the angle between section plane and cylinder core. This observation was used to estimate the fibre direction, *e.g.*, by Zhu *et al.* (1997). However, a fibre direction is not uniquely determined by the corresponding cross-section. To overcome this problem, Clarke *et al.* (1995) and Eberhardt and Clarke (2001) used confocal laser scanning microscopy to determine fibre directions by tracking individual fibres

in glass fibre reinforced polymers through a depth of up to 150  $\mu\text{m}$ . Nevertheless, this type of stereological reconstruction of the three-dimensional fibre directions from planar sections is error-prone in particular for curved fibres or for straight fibres which are parallel to the section plane. These problems can be avoided by computed micro-tomography ( $\mu\text{CT}$ ), which is capable to fully reconstruct the three-dimensional microstructure of fibre reinforced materials.

Recently, a number of quantities characterising fibre direction distributions as well as a wide range of image analysis algorithms for computing these quantities from 3D data obtained by  $\mu\text{CT}$  have been proposed. The rose of directions, *i.e.*, the probability density function of the direction distribution, can be obtained via the inverse cosine transform of data either obtained from so-called generalised projections onto subspaces (Ohser and Schladitz, 2009) or from counts of fibre sections in section planes (Kiderlen and Pfrang, 2005; Riplinger and Spiess, 2012). While the former method is highly efficient with a low directional and high lateral resolution, the latter one features a high directional resolution and a low lateral resolution. Ohser *et al.* (1998) pointed out the mutual exclusion of increasing both, directional and lateral resolution

for this class of algorithms. In the present paper, estimating the rose of directions is not considered, since in contrast to the methods that we will use here, it does not allow for a local analysis of fibre systems.

The segmentation of fibre profiles either in section planes is a non-trivial image processing task. In order to compute fibre direction distributions without this tedious pre-processing, some authors have proposed to reduce the computation of fibre direction distributions to the computation of local fibre directions in individual pixels. As all of these methods average over pixels to obtain local directional estimates, they can be characterised as algorithms for a volume-weighted fibre direction estimation.

Robb *et al.* (2007), Wirjadi (2009), and Wirjadi *et al.* (2009) test for each fibre pixel the filter response of anisotropic, prolate Gaussian filters with major principal axis from a finite set of directions, see the section “Methods” below for details. As we will show, such an approach is viable but of limited accuracy due to the strongly restricted number of directions that can be considered in practice due to runtime limitations. Sandau and Ohser (2007) proposed the so-called chord length transform (CLT) which assigns to each fibre point the chord of maximum length covered by the fibre. The direction of this chord is used as an estimate of the local fibre direction. The CLT will not be considered within the present paper. It requires testing a certain number of chord directions, entailing the same problematic dependence between accuracy and runtime as observed for the anisotropic Gaussian filter method. The approach of Altendorf and Jeulin (2009) can be seen as an advanced CLT as it is based on the CLT idea but refines estimation of the local fibre direction by computing it from the main axis of inertia. This latter approach will be summarised and evaluated below.

Choosing a finite number of test directions is not required at all when considering partial derivatives of the local grey value structure along fibres. Krause *et al.* (2010) accumulate gradient information in structure tensors and derive the local fibre direction from the eigendecomposition of these tensors. Similarly, the Hessian matrix of second partial derivatives yields the local fibre direction, as this corresponds to the direction of lowest grey value curvature as observed by Frangi *et al.* (1998); Tankyevych *et al.* (2009). Both of these approaches based on partial derivatives will be described in more detail in the following section “Methods”.

This paper contributes to the development of fibre direction estimation by subsuming the previously proposed algorithms in a common framework and

by showing how the volume-weighted fibre direction distribution relates to other quantities characterising directional features of fibre structures. Lastly, our numerical results on simulated data may be used as a guideline for practitioners seeking suitable analysis algorithms.

## MATERIALS AND METHODS

### ORIENTATION ANALYSIS

In this section, we introduce methods that allow us to characterise the directional distributions of fibre systems in composite materials based on image data. In particular, we define the volume-weighted directional distribution, derive the orientation tensors, and describe the four methods for estimating the fibre direction in each pixel. Let  $\Phi$  denote a macroscopically homogeneous (but anisotropic) random fibre system in  $\mathbb{R}^3$  following the definition by Mecke and Nagel (1980); Nagel (1983), that is  $\Phi$  is a random system of rectifiable curves.

In our setting, the thickness of the fibres is not negligible. We will therefore address the random set  $\Xi = \Phi \oplus B_r$  as the fibre system while calling  $\Phi$  the fibre core system. That is, the random fibre system  $\Xi$  is derived from the random fibre core system  $\Phi$  by dilation with the ball  $B_r$  of radius  $r > 0$ . Note that for a wide range of fibre-reinforced composites, *e.g.*, most glass and carbon fibre-reinforced polymers and steel fibre-reinforced concretes, the fibre radius  $r$  is known from the production process. Therefore, we will assume fibres with a circular cross-section and constant diameter  $2r$  throughout this paper. The fibre system  $\Xi$  may be sufficiently smooth, and self-intersections may not occur. More precisely, we suppose that there is an  $\varepsilon > 0$  such that  $\Xi$  is morphologically closed w. r. t.  $B_\varepsilon$ ,

$$(\Xi \oplus B_\varepsilon) \ominus B_\varepsilon = \Xi. \quad (1)$$

Condition Eq. (1) ensures that the direction of the fibre core system is uniquely defined in each point within the fibre system. Moreover, being morphologically closed means that the local curvature of the fibre core system must be less than  $1/r$  and thus in particular that the fibre surfaces are not rough.

Finally, assume that fibres are fibres in the sense that they are longer than wide, that is, their length is significantly larger than their diameter  $2r$ .

For a point  $y$  in the fibre core system  $\Phi$ , denote by  $v(y)$  the tangent direction. We now define the local fibre direction  $v(x)$  of a point  $x$  in the fibre system  $\Xi$ .

This direction corresponds to the fibre core system's tangent direction in the point that is closest to  $x$ , i. e.,  $v(x) = v(y)$  with  $y = \operatorname{argmin}_{y \in \Phi} \|x - y\|$ . This point  $y$  is unique due to the assumption Eq. (1) on  $\Phi$  and the diameter of the fibres in  $\Xi$  made above. The vectors  $v(x)$  form a random vector field. Note that we need not to consider the orientation, i. e., the sign of  $v(x)$ , for its choice in a fibre point  $x \in \Xi$  is ambiguous. Thus we consider the set  $S_+^2$  of non-oriented directions that is equivalent to the upper hemisphere.

Disregarding noise and artefacts for the moment, a tomographic reconstruction yields a 3D image  $f$  which is an observation of the fibre system  $\Xi$  of the form  $f(x) = 1_\Xi(x)$ , where  $1_\Xi$  denotes the indicator function of  $\Xi$ . Now, assume for the moment that we were able to compute the random vector field  $v(x)$  at every point  $x \in \Xi$  in the fibre system from an image  $f$ . In the current context, we are interested in the fibre direction distribution in the typical fibre point of the fibre system. Then the mean  $R$  over local directions  $v(x)$  in a compact window  $W \subset \mathbb{R}^3$  with volume  $\operatorname{vol}(W) > 0$ ,

$$R(A) = \frac{1}{2\pi \mathbb{E} \operatorname{vol}(\Xi \cap W)} \mathbb{E} \int_{\Xi \cap W} 1_A(v(x)) dx, \quad (2)$$

where  $A \subset S_+^2$  is a measurable set of directions, is a probability measure. The expectation in Eq. (2) should be understood with respect to the fibre system  $\Xi$ . The distribution  $R$  is *volume-weighted*, since it averages over all points occupied by the fibre system  $\Xi$ .

For systems of fibres with variable thickness, the just defined direction distribution  $R$  is a so-called volume-weighted one. More precisely,  $R(A)$  is the direction distribution function of the typical point of  $\Xi$ . Analogously, a surface-weighted direction distribution is the direction distribution of the typical point on the surface  $\partial\Xi$  of  $\Xi$  and, finally, the direction distribution of the core system  $\Phi$  is the length-weighted direction distribution as defined by Mecke and Nagel (1980). These distributions can differ considerably. In our setting of constant fibre thickness however, the volume-, surface-, and length-weighted fibre direction distributions are identical (up to edge effects resulting from contributions of the fibre ends).

To summarise, if we were given access to the random vector field  $v(x)$  and to the set of points occupied by the fibre system  $\Xi$  in an observed and possibly degenerated image  $f$ , the volume-weighted fibre direction distribution would be available with Eq. (2).

## ORIENTATION TENSORS

Instead of the probability measure  $R$ , it is often more convenient to work with the moments of  $R$ , the so-called *orientation tensors* as defined by Advani and Tucker (1987). Let  $u_i$  denote the  $i$ th component of some normalised direction vector  $u$ . Then the second and fourth order orientation tensors are defined as  $A^{(2)} = (a_{ij})$  and  $A^{(4)} = (a_{ijkl})$  with

$$a_{ij} = \int_{S_+^2} u_i u_j R(du),$$

$$a_{ijkl} = \int_{S_+^2} u_i u_j u_k u_l R(du), \quad i, j, k, l = 1, 2, 3.$$

Tensors of orders other than two and four can of course be defined in a similar way. In order to highlight the relevance of orientation tensors, we follow the arguments of Advani and Tucker (1987): Material properties such as the behaviour under mechanical stress are usually modeled in continuum, where a continuous, homogeneous material is assumed, rather than a two-phase medium such as fibre-reinforced polymers. This process requires averaging of the properties of the two materials over the direction distribution  $R$ . The average of a material property  $T$  over all space directions is denoted by  $\langle T \rangle$ ,

$$\langle T \rangle = \int T(u) R(du). \quad (3)$$

For computational efficiency, it is desirable to replace the integral over the hemisphere in Eq. (3) by some simplified expression. This is where orientation tensors fit in. For instance, under some symmetry assumptions for the material (called transverse isotropy by Advani and Tucker (1987)), the second-order, tensor-valued material property tensor  $T^{(2)}$  is a sufficient description of  $\langle T \rangle$ , and can be decomposed as

$$T^{(2)} = (T_{ij}) \quad \text{with} \quad T_{ij} = b_1 a_{ij} + b_2 \delta_{ij},$$

where  $b_1$  and  $b_2$  are scalars, and  $\delta_{ij}$  is the Kronecker delta. Depending on the symmetries, similar relations can also be derived between fourth-order tensor-valued properties and the fourth-order orientation tensor  $A^{(4)}$ . Examples for second-order tensor-valued properties are thermal expansion and thermal conductivity, while elastic stiffness or viscosity can be described as fourth-order tensors (Advani and Tucker, 1987; Bunge, 1993). Thus, orientation tensors play a central role in the simulation of material properties.

Beyond their use in continuum modeling, orientation tensors, especially the eigendecomposition of  $A^{(2)}$ , allow for intuitive compact descriptions of the shape of the direction distribution  $R$ . For

instance, the eigenvector to the largest eigenvalue  $\lambda_{\max}$  of  $A^{(2)}$  corresponds to the mean fibre direction. Furthermore, ratios between  $a_{ij}$ 's eigenvalues can be used to characterise the anisotropy of  $R$ , see Fisher *et al.* (1987). One such useful characteristic is the anisotropy factor  $\alpha = 1 - \lambda_{\min}/\lambda_{\max}$ . This degree of anisotropy  $\alpha$  is zero for the isotropic fibre direction distribution.  $\alpha = 1$  means that the fibre direction distribution is concentrated on a great circle. In the latter case,  $\alpha$  does however not differentiate between a uniaxial or an isotropic distribution within the plane determined by the great circle.

These two scenarios motivate our search for methods that compute the orientation tensors  $A^{(2)}$  and  $A^{(4)}$  directly from an image  $f$ . We follow the same concept as for the directional fibre distribution in Eq. (2) and replace the integral w. r. t. the unknown probability measure  $R$  in Eq. (3) by a sample over local fibre direction vectors  $v(x)$  with components  $v_i(x)$ . This yields

$$a_{ij} = \frac{1}{\mathbb{E}\text{vol}(\Xi \cap W)} \mathbb{E} \int_{\Xi \cap W} v_i(x)v_j(x) dx, \quad (4)$$

$$a_{ijkl} = \frac{1}{\mathbb{E}\text{vol}(\Xi \cap W)} \mathbb{E} \int_{\Xi \cap W} v_i(x)v_j(x)v_k(x)v_\ell(x) dx. \quad (5)$$

for the components of the second and fourth order orientation tensors.

The remainder of this paper is dedicated to the introduction of algorithms for estimating  $R$  and the derived characteristics from image data of fibre-reinforced composites, to their interpretations, and to the experimental evaluation and application of those methods.

## IMAGE BINARISATION

From an image processing perspective, the quantities introduced above simplify the problem at hand. Methods for computing the fibre direction distribution proposed so far usually required precise segmentations of fibres either in 2D (Clarke *et al.*, 1995; Lee *et al.*, 2002; Kiderlen and Pfrang, 2005), or in 3D (Yang and Lindquist, 2000; Tan *et al.*, 2006). In contrast to that, Eq. (2) and Eq. (5) merely require the fibre system  $\Xi$ . That is, these estimators do not require a segmentation of individual fibres, but only a segmentation of the complete fibre system. A binarisation of an image is a separation of its pixels into two disjoint sets. In the present context, it yields an estimation of the set of pixels covered by the fibre system and its complement.

This can be achieved using standard image processing methods. From our experience, sufficient binarisations of tomographic reconstructions of fibre reinforced polymers can easily be achieved using some low-pass noise reduction filters and a global grey value threshold. To demonstrate that this is true for images encountered in practice, consider the binarisation of the  $\mu$ CT image of a glass fibre-reinforced polymer in Fig. 1. Here, a simple smoothing filter ( $3 \times 3 \times 3$  discrete Gaussian) and a global threshold value derived from the grey value distribution in the image were used. While such a binarisation is not sufficient to segment individual fibres, it is sufficient as an estimate of the fibre system  $\Xi$  required in the present paper.

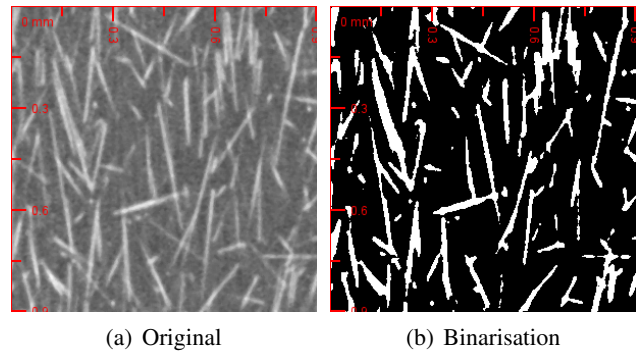


Fig. 1. *Binarisation of the fibre system of a glass fibre-reinforced polymer (GFRP) imaged at  $3 \mu\text{m}$  pixel size. Further results regarding this dataset will be presented in the Application section below. Here, a  $3 \times 3 \times 3$  discrete Gaussian filter is followed by a simple global threshold.*

Note that the thus derived binarisation might locally not be good enough to fulfill the condition Eq. (1). Thus, some pixels of the fibre system can not be assigned uniquely to a fibre core. However, as this problem typically occurs where parallel fibres touch, it does not cause large estimation errors.

For all algorithms introduced below, we will use such image binarisations as an estimation of  $\Xi$  in order to restrict the evaluation of fibre directions to pixels belonging to the fibre system.

## ESTIMATION OF LOCAL FIBRE DIRECTIONS

Local directional information has widely been used in the image processing literature. The moments of inertia have been used as features for object and pattern recognition for a very long time, see *e.g.*, Hu (1962); Prokop and Reeves (1992), and more recently to analyse and segment images of fibrous materials by Altendorf and Jeulin (2009; 2011) and Altendorf *et al.* (2012).

Anisotropic linear filters, and the directional information contained in first and second order derivatives have been exploited for image filtering: Anisotropic Gaussian filters were shown to be suitable for adaptive smoothing of diffusion tensor magnetic resonance data (DT-MRI), *e.g.*, by Lee *et al.* (2006). The structure tensor (a  $3 \times 3$  matrix of smoothed pairwise products of first partial derivatives) is used in diffusion filters, *e.g.*, coherence enhancing diffusion filtering by Weickert (1999). Finally the Hessian matrix (a  $3 \times 3$  matrix of partial second derivatives) has been proposed as a suitable tool in algorithms for smoothing images of tubular structures, *e.g.*, by Frangi *et al.* (1998).

Next, we will describe algorithms that use exactly these concepts. The difference here lies in the fact that we will use the results of these algorithms directly as estimates for the random vector field  $v(x)$ , rather than as an intermediate result for subsequent image smoothing.

Three of the algorithms that will be introduced in the following sections employ a Gaussian smoothing. We will choose the known fibre radius  $r > 0$  for the Gaussian kernel parameter  $\sigma$ . This choice is backed up by results from linear scale space theory Lindeberg (1994), where it is known that the standard deviation of the Gaussian kernel is a measure for spatial scale.

### Maximum response of anisotropic Gaussians

Let  $g_u$  denote the mask of an anisotropic 3D linear filter with a prolate shape,  $u$  the direction of its longest principal axis, and  $*$  convolution. Then the filter response  $(g_u * f)(x)$  assumes its maximum when  $u$  is aligned to the preferred fibre direction in a point  $x \in \mathbb{E}$ . This observation leads to an algorithm for computing the random vector field  $v(x)$ : At every point  $x \in \mathbb{E}$ , find the direction  $v$  that maximises the filter response,

$$v(x) = \operatorname{argmax}_{u \in S_+^2} (g_u * f)(x). \quad (6)$$

Since we must maximise over the upper hemisphere  $S_+^2$  in every pixel, the maximisation in Eq. (6) can be computationally expensive. Therefore, we use anisotropic Gaussian filters, for which a fast implementation of the convolution was obtained by Lampert and Wirjadi (2006). Anisotropic Gaussian filters have the form

$$g_u(x) = \frac{1}{(2\pi)^{3/2} \sqrt{\det \Sigma_u}} \exp\left(-\frac{1}{2} x^T \Sigma_u^{-1} x\right), \quad \text{for } x \in \mathbb{R}^3. \quad (7)$$

Here,  $\Sigma_u$  denotes the positive definite  $3 \times 3$  covariance matrix determining the shape of the filter mask. To implement Eq. (6), we use a mask for which all non-empty level sets have the shape of prolate spheroids. In this case,  $\Sigma_u$  has four degrees of freedom. Different useful parameterisations of  $\Sigma_u$  exist. We use spherical polar coordinates to define the fibre direction  $v(x)$ , thus the corresponding parameterisation of  $\Sigma_u$  is given.

Let  $(\varphi, \vartheta)$  denote the spherical polar coordinates of  $u$ ,  $\vartheta \in [0, \pi]$  the colatitude and  $\varphi \in [0, 2\pi]$  the longitude. Furthermore, let  $r = \sigma_1 = \sigma_2 > 0$  denote the standard deviation of the Gaussian kernel Eq. (7) in the two directions orthogonal to  $u$ , and let  $\sigma_3 \gg \sigma_1$  denote the standard deviation in direction  $u$ . Then we get the following parameterisation for the covariance matrix:

$$\Sigma_u = R_{\varphi, \vartheta} \begin{pmatrix} \sigma_1^2 & 0 & 0 \\ 0 & \sigma_1^2 & 0 \\ 0 & 0 & \sigma_3^2 \end{pmatrix} (R_{\varphi, \vartheta})^T,$$

with

$$R_{\varphi, \vartheta} = \begin{pmatrix} \cos \varphi \cos \vartheta & -\sin \varphi & \cos \varphi \sin \vartheta \\ \sin \varphi \cos \vartheta & \cos \varphi & \sin \varphi \sin \vartheta \\ -\sin \vartheta & 0 & \cos \vartheta \end{pmatrix}.$$

For alternative parameterisations of  $\Sigma_u$ , see, *e.g.*, Lampert and Wirjadi (2006); Wirjadi (2009).

In order to implement the maximisation in Eq. (6), we sample  $S_+^2$  in  $m$  points following the numerical scheme of Fliege and Maier (1999) for  $S^2$ , as it is readily modified to yield  $m$  directions  $u_i \in S_+^2$  ( $i = 1, \dots, m$ ) free of edge effects. This results in a set of  $m = 98$  points on the upper hemisphere with nearest neighbour distances between  $12.7^\circ$  and  $15^\circ$ . We refer to Wirjadi (2009) for details, where also a list of these vectors can be found.

In summary, an algorithm for estimating the random vector field  $v(x)$  is derived by choosing in each pixel  $x$  the direction  $v(x)$  that locally maximises the result of the convolution of image  $f$  with a set of anisotropic Gaussian filters  $g_{u_i}$ ,  $i = 1, \dots, m$ . Of course, the achievable accuracy of this method depends on the set of pre-computed directions that are probed, and therefore directly influences the runtime.

### Main axis of inertia

The basic idea of this method of Altendorf and Jeulin (2009) is essentially the same as the one exploited by the just described method: Locally, a fibre can be approximated by a prolate rotation ellipsoid whose shorter half-axis length corresponds to the fibre radius while the direction of the longer axis is the local fibre direction. Altendorf and Jeulin (2009) derive the

ellipsoid of inertia from directed distance transforms. The main axis of the ellipsoid then yields the local fibre direction.

More precisely, from the result of directed distance transforms in the 26 spatial directions given by the maximal pixel adjacency, the moments and axes of inertia are computed. Start with a binarisation of the fibre system achieved *e.g.*, by a simple global threshold as described above. Let  $\ell \in L = \{-13, \dots, -1, 1, \dots, 13\}$  index the discrete directions  $v_\ell$  given by the maximal pixel adjacency in a way that the symmetry  $v_\ell = -v_{-\ell}$  holds. Denote by  $d_\ell(x)$  the distance from  $x$  to the next background pixel in direction  $v_\ell$ . That is,  $d_\ell(x)$  is the result of the directed distance transform. Then the sum of the distances  $d_\ell(x) + d_{-\ell}(x)$  yields the length of the chord through  $x$  in direction  $v_\ell$ . The moments of inertia  $M_{ijk}(x)$  are derived from the endpoints of the centralised chords  $P_\ell(x) = \frac{1}{2}(d_\ell(x) + d_{-\ell}(x))v_\ell$  by

$$M_{ijk}(x) = \sum_{\ell \in L} (P_{\ell,0}(x))^i (P_{\ell,1}(x))^j (P_{\ell,2}(x))^k \quad \text{for } i, j, k = 0, 1, 2,$$

where  $P_{\ell,m}$ ,  $m = 0, 1, 2$  denote the components of the  $P_\ell$ . Finally, the inertia tensor is given by

$$M(x) = \frac{1}{26} \begin{pmatrix} M_{200}(x) & M_{110}(x) & M_{101}(x) \\ M_{110}(x) & M_{020}(x) & M_{011}(x) \\ M_{101}(x) & M_{011}(x) & M_{002}(x) \end{pmatrix}.$$

The eigenvector of  $M(x)$  corresponding to its largest eigenvalue is the main axis of inertia, or an estimate the local fibre direction  $v(x)$  in  $x$ .

The direction discretisation emphasizes the 26 used directions and thus results in a systematic error. Altendorf and Jeulin (2009) derived a correction reducing both the maximal and the mean error drastically from about  $10^\circ$  to less than  $5^\circ$  and from  $6.4^\circ$  to  $1.3^\circ$ , respectively. Introduce the empirical correction term

$$t(\beta) = \begin{cases} -0.2 \sin(\pi(4\beta/\pi)^{0.424}), & \text{if } \beta < \pi/4, \\ 0, & \text{otherwise.} \end{cases}$$

The corrected direction estimate  $v'$  is

$$v' = v + \sum_{\ell \in L} t(\arccos(v_\ell v)) \|v_\ell \times v\|. \quad (8)$$

Note that  $\arccos(v_\ell v)$  is the angle formed by  $v$  and  $v_\ell$  and  $\|v_\ell \times v\|$  is the length of the orthogonal projection of  $v_\ell$  on the plane perpendicular to  $v$ . As mentioned above, the described version of the algorithm starts

with a binarisation. This can be avoided by utilising grey-value pseudo-distances as described by Altendorf and Jeulin (2009).

## The structure tensor

The fibre direction  $v$  is orthogonal to the fibre surface normals, that is, to the gradient direction in the image. To account for the circular cross-section of the fibres, we operate on images that have been smoothed using an isotropic Gaussian filter. As argued above, we set  $\sigma = r$ , as has also been done by Krause *et al.* (2010). That means, the gradient directions at size scale  $r$  are determined. A general problem with gradients in image data is noise, due to the fact that they are implemented by difference filters. Therefore one needs a mechanism for smoothing edge directions. This can be achieved by considering the tensor product of gradients,  $(\nabla f)(\nabla f)^T$ , a positive semi-definite matrix with at most one non-zero eigenvalue. The elements of this matrix are smoothed spatially using a second isotropic Gaussian filter  $g_\rho$ :

$$S_{\sigma,\rho} = g_\rho * \left( (\nabla f * g_\sigma) \cdot (\nabla f * g_\sigma)^T \right), \quad (9)$$

where the outer convolution with  $g_\rho$  is applied component-wise, thus resulting in a matrix with more than one non-zero eigen value, in general. The resulting  $S_{\sigma,\rho}$  is known as the structure tensor and has successfully been used *e.g.*, in the context of coherence enhancing diffusion filtering by Weickert (1999). Its eigendecomposition describes the local image texture. Especially, the eigenvector with respect to the smallest eigenvalue of  $S_{\sigma,\rho}$  corresponds to the direction with coherent local grey values, *i.e.*, it points in the direction where the gradient is minimal. In the context of the present paper, this is the required local fibre direction  $v(x)$ , as the fibre boundaries are expected to produce large gradients.

From our experience, it is of particular importance to choose the pre-smoothing parameter  $\sigma$  correctly when applying this algorithm. As it uses gradient information, it may detect edge structures – instead of fibres – if the fibre diameter does not fit the chosen value of  $\sigma$ .

## Hessian matrix

A further method for estimating local fibre directions is the use of the Hessian matrix. While gradients contain information on the direction of edges, second derivatives are known to describe curvature and therewith the direction of ridge-like structures (Eberly *et al.*, 1994). Here again, one needs to handle noise, and therefore we define the Hessian

matrix  $H_\sigma$  computed from a smoothed image  $f$  as

$$H_\sigma = (\nabla\nabla^T)(f * g_\sigma) \quad (10)$$

As outlined above, an appropriate choice for the smoothing parameter is  $\sigma = r$ . Using this value, structures thinner than  $2\sigma$  are suppressed by the smoothing, see the thinner bar in Fig. 2b. On the other hand, a much smaller  $\sigma$  results in erroneous direction estimates in pixels close to the fibre cores.

Our assumption on the fibre system Eq. (1) implies in particular that the curvature of the fibres is small compared to the inverse fibre radius. Thus the eigenvector of  $H_\sigma$  with respect to the smallest (in magnitude) eigenvalue is an estimator of the local fibre direction. Similar observations have previously been made by Eberly *et al.* (1994) and Frangi *et al.* (1998).

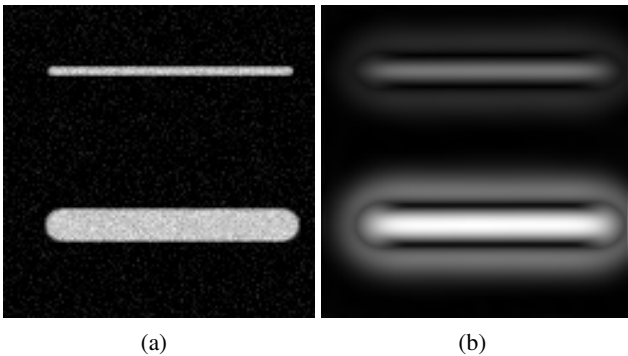


Fig. 2. Demonstration of the effect of smoothing on the largest (in magnitude) eigenvalue of the Hessian matrix in a 2D example. (a) Two bars of different width in some additive Gaussian noise, (b) The largest (in magnitude) eigenvalue of the Hessian  $H_\sigma$  in every pixel. The parameter  $\sigma$  has been set to correspond to half the width of the thicker bar.

## RESULTS

The applicability of the four different algorithms for directional analysis of fibre systems is known from the literature: The Gaussian filter method has been applied to  $\mu$ CT images of glass and carbon fibre reinforced composites by Robb *et al.* (2007), Wirjadi (2009) and Wirjadi *et al.* (2009), the main axis of inertia to glass fibre reinforced composites and collagen fibres by Altendorf and Jeulin (2009) and Altendorf *et al.* (2012), the Hessian matrix was applied for image smoothing of medical images by Frangi *et al.* (1998), and the structure tensor was applied to images of short fibre-reinforced C/SiC and glass fibre-reinforced composites by Krause *et al.* (2010). In the following, we compare the four algorithms, with the focus on synthetic data.

## RUNTIMES

All four method's complexity is  $\mathcal{O}(n)$ , where  $n$  is the number of pixels, independent of the smoothing parameters  $\sigma$  and  $\rho$ . For the anisotropic Gaussian filter method, this is achieved by making use of the filter separation scheme of Lampert and Wirjadi (2006). Gaussian filtering can be performed using  $\mathcal{O}(n)$  operations using recursive algorithms as *e.g.*, Young and van Vliet (1995). The 1D distance transform required as subroutine of the method of axis of inertia is also known to be of linear time complexity (Rosenfeld and Pfaltz, 1966). Our experimental validation of this linear dependency is based on volumes containing one cylinder with constant radius (5 pixels) and increasing lengths such that the volume density is 1%, see Fig. 3.

The results in Fig. 3 confirm the linear complexity, but show also that the constants ignored in  $\mathcal{O}$ -notation differ considerably, here. Especially the anisotropic Gaussian filter algorithm, which relies on sampling  $S_\pm^2$  in  $m$  points, is drastically slower than the other three methods. The Hessian matrix method turns out to be the fastest one, which can be explained by the additional spatial smoothing using parameter  $\rho$  that is applied on all six unique elements of the gradient's tensor product to compute the structure tensor, *cf.* Eq. (9).

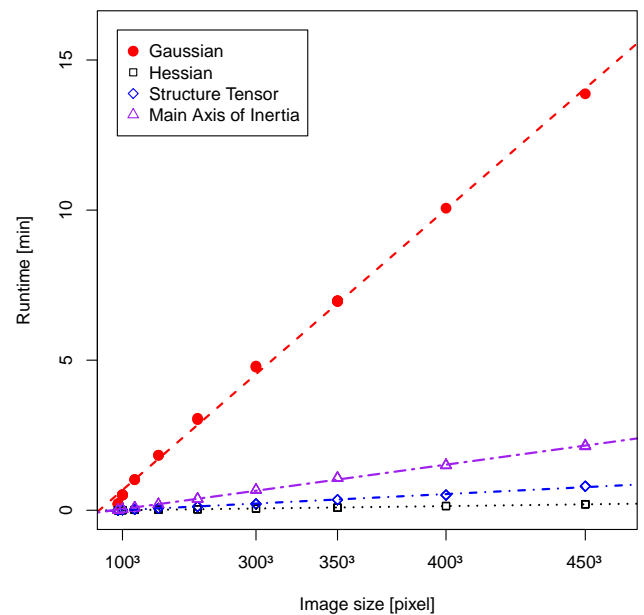


Fig. 3. Runtimes of the four algorithms for image sizes between  $50^3$  and  $450^3$  on an Intel Xeon X5675 at 3.07 GHz. The number of sampling points for the Gaussian filter method is  $m = 98$ , the smoothing parameters are  $\sigma = 5$  and  $\rho = 1$  in all cases.

## SYSTEMATIC ERRORS ON SIMULATED DATA

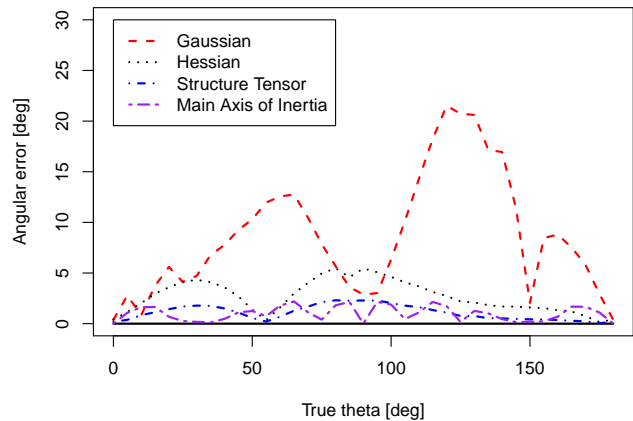
The usage of simulated image data is the only way of measuring an image analysis algorithm's accuracy. To measure accuracy, we use the difference angle  $\delta = \arccos v^T \hat{v}$ , where  $\hat{v}$  denotes the mean fibre direction obtained as the eigenvector corresponding to the largest eigenvalue of the second order orientation tensor in Eq. (4).

All image data used in the present section consists of  $128 \times 128 \times 128$  pixels, containing one single cylinder with radius 5 pixels and a length of 80, centered in the image. The principal direction  $v$  of the cylinder is used as a free parameter in the following experiments.

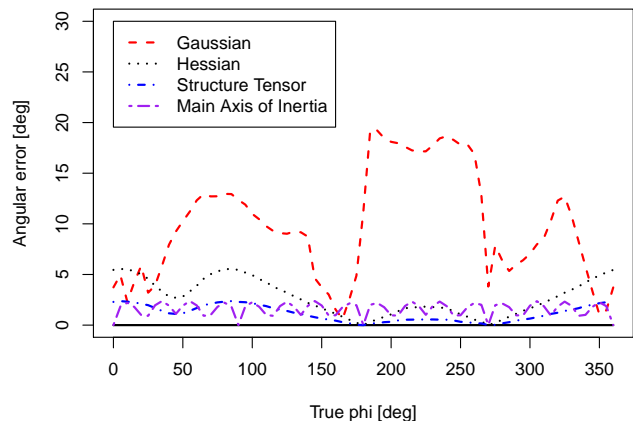
We first evaluate the four algorithms' accuracy depending on  $v$  in order to analyse discretisation effects. The results are shown in Fig. 4 which illustrates the systematic errors, where  $v = (\vartheta, \varphi)$  is decomposed into its polar coordinate representation with the colatitude  $\vartheta \in [0, \pi]$  and longitude  $\varphi \in [0, 2\pi)$ . By keeping one angle fixed and varying the other, we can assess the methods' accuracy in this noise-free setting. Note that strictly speaking, the results in Fig. 4(a) for  $\vartheta > \pi/4$  lie on the lower hemisphere. We chose this representation here for an easier parameterization, nevertheless. By symmetry, these results ( $\varphi = \pi/4$  and  $\vartheta > \pi/4$ ) can easily be mapped to the upper hemisphere by mirroring the corresponding vectors on the origin.

The Hessian and the structure tensor as well as the main axis of inertia methods are capable of measuring the cylinder's major axis direction within an error margin of only a few degrees. When using the method based on anisotropic Gaussian filtering, on the other hand, maximal errors are expected when the cylinder's direction is far from one of the  $m$  samples on the upper hemisphere. Thus, accuracy of the Gaussian filter method depends on the number of sampling directions, *i.e.*, it depends on the discretisation of  $S_+^2$  in Eq. (6), where a "uniform" distribution of  $m$  points on  $S_+^2$  is a crucial problem. Clearly, with increasing  $m$ , the accuracy of estimation, but also the runtime increase. This is a clear disadvantage of the Gaussian filter method. Fig. 4 shows that for some fibre directions, measurement errors from the Gaussian method even exceed the hemisphere's maximal sampling grid distance of  $15^\circ$  reported by Wirjadi (2009). It is quite remarkable that the main axis of inertia method circumvents this trap by the empirical correction Eq. (8) although being based on just 13 directions.

To give an impression of the algorithms' robustness with respect to noise, a further experiment is performed. Straight cylinders model fibres, where the directions  $v$  are chosen independently identically distributed in  $S_+^2$ . To the binary images of the cylinders, Gaussian noise with variance  $s^2$  is added. This allows to plot the resulting accuracy  $\delta$  over the noise variance  $s^2$  in Fig. 5.

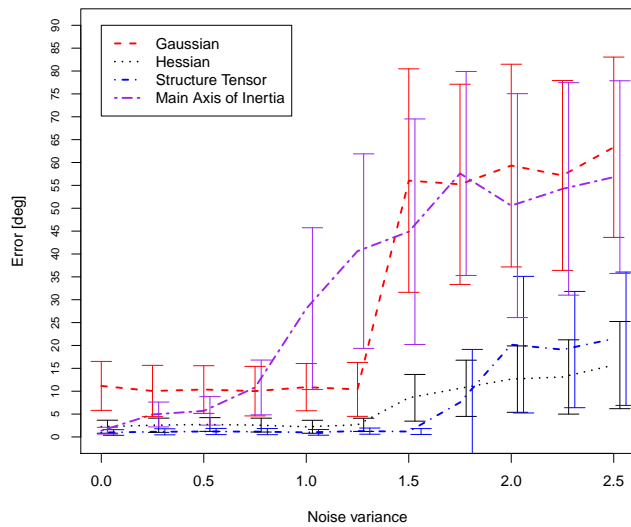


(a) Cylinders parallel to the  $xz$ -plane ( $\varphi = 0$ ). The component  $\vartheta$  of the axis direction is varied.

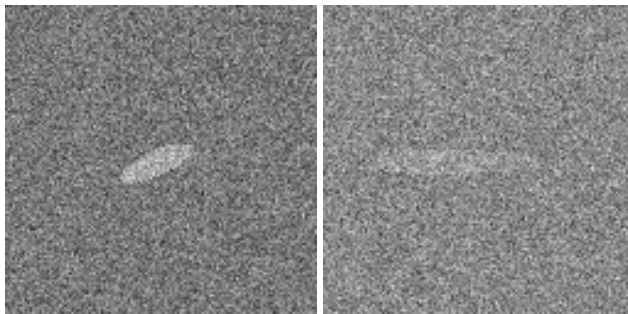


(b) Cylinders parallel to the  $xy$ -plane ( $\vartheta = \pi/2$ ). The component  $\varphi$  of the axis direction is varied.

Fig. 4. *Systematic error of fibre direction estimation for cylinders with varying principal directions: Angular error  $\delta$  of the mean fibre direction computed using the four considered algorithms from the true, known fibre direction. The direction of the cylinder's principal axis is given in polar coordinates. The smoothing parameter  $\sigma$  is fixed to the cylinder's radius  $r$ ,  $\sigma = r = 5$ ,  $\rho = 1$  and  $m = 98$ .*



(a) Angular error of the mean fibre direction as a function of noise variance  $s^2$



(b) Examples (left:  $s^2 = 0.5$ , PSNR=6.0 dB; right:  $s^2 = 1.5$ , PSNR=-3.5 dB)

Fig. 5. Errors of estimated fibre direction from 100 realisations of uniformly distributed directions of the cylinder under noise. Independent, identically distributed, additive Gaussian noise with given variance is used. The fibre radius is fixed to  $r = 5$ ,  $\sigma = r$ ,  $\rho = 1$  and  $m = 98$ .

The results in Fig. 5 show once again that in noise-free and low noise situations, the Gaussian filter method's accuracy is between  $10^\circ$  and  $12^\circ$ . For low noise levels, the main axis of inertia method's error is well below  $10^\circ$  while at a noise variance of 0.75, it starts to behave worse than the Gaussian filter method. This is due to the underlying distance measurements being easily distorted by noise. Switching to the grey value distance version of the algorithm does not change the result significantly. The two gradient-based methods, on the other hand, achieve accuracies of a few degrees. All methods' accuracy decreases rapidly as the noise variance exceeds 1.5 – which corresponds to a peak signal-to-noise ratio (PSNR) of -3.5 dB for the test data used here. The accuracy of the Hessian and of the structure tensor methods are the same (within one standard deviation for most values of  $s^2$ ).

In summary, the experiments on synthetic data presented in this section show that the Hessian matrix and structure tensor-based estimators are faster than the main axis of inertia which is in turn faster than the Gaussian filter-based approach, under all tested fibre directions  $v$  and all tested noise variances  $s^2$ . In terms of precision, the three methods apart from the Gaussian filter method performed equally well in our noise-free experiments, with deviations below  $5^\circ$  under all tested fibre directions  $v$ . The main axis of inertia is very noise sensitive. Thus, we finally opt for the faster of the two grey value derivative based algorithms, *i.e.*, the Hessian matrix, in the following application examples.

## APPLICATION

In this section, we apply the developed methods to two glass fibre reinforced polymer samples and a carbon fibre reinforced polymer sample. These two types of composites which are most common in industrial applications, today.

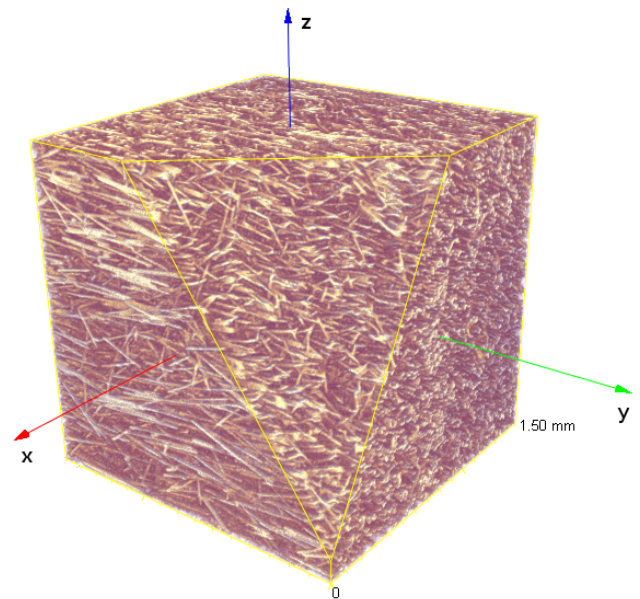


Fig. 6. Volume rendering of a  $(1.5\text{ mm})^3$  specimen of glass fibre reinforced polymer, imaged at  $3\mu\text{m}$  spatial resolution using a laboratory X-ray computed tomography system.

Fig. 6 shows the volume rendering of a computed tomography (CT) reconstruction of a glass fibre-reinforced polymer (GFRP) specimen with 30% glass fibres (measured by weight). With a known fibre diameter of  $12\mu\text{m}$ , the second order orientation tensor of the glass fibre reinforced polymer is estimated from that data as

$$A^{(2)} = \begin{pmatrix} 0.205 & -0.020 & -0.017 \\ -0.020 & 0.605 & 0.013 \\ -0.017 & 0.013 & 0.190 \end{pmatrix}. \quad (11)$$

From the maximum entry in the second diagonal element of  $A^{(2)}$ , we can already tell that most fibres are parallel to  $y$ , which we can also compute via an eigendecomposition of this matrix, yielding  $(-0.0505, 0.998, 0.0335)^T$  as mean fibre direction.

While the previously investigated GFRP-sample was rather homogeneous and the fibres well separated, the Hessian fibre orientation algorithm will be applied to a more complex carbon fibre reinforced polymer (CFRP) sample now. The image data was obtained by high-quality  $\mu$ CT at beamline ID19 of the ESRF in Grenoble. The spatial resolution is  $0.7\mu\text{m}$ . In a first step, we can compute the overall orientation tensor in the same way as for the GFRP sample above.



Fig. 7. *Layers of differently oriented carbon fibres in a reinforced polymer sample from the aviation industry. The layers have been segmented in terms of their angular difference to the global mean fibre direction.*

$$A^{(2)} = \begin{pmatrix} 0.200 & -0.003 & -0.012 \\ -0.003 & 0.284 & 0.020 \\ -0.012 & 0.020 & 0.516 \end{pmatrix}. \quad (12)$$

Yet, the global tensor in Eq. (12) is not representative of the entire specimen. If instead of averaging over the entire image, we pick  $W$  in Eq. (4) as a cube with side length  $266\mu\text{m}$  and compute local tensors in cubes that cover the image entirely (tiling), we will end up with

different results such as the following two examples:

$$A_1^{(2)} = \begin{pmatrix} 0.207 & 0.012 & -0.041 \\ 0.012 & 0.178 & 0.031 \\ -0.041 & 0.031 & 0.614 \end{pmatrix},$$

$$A_2^{(2)} = \begin{pmatrix} 0.198 & 0.009 & -0.009 \\ 0.009 & 0.527 & 0.032 \\ -0.009 & 0.032 & 0.276 \end{pmatrix}.$$

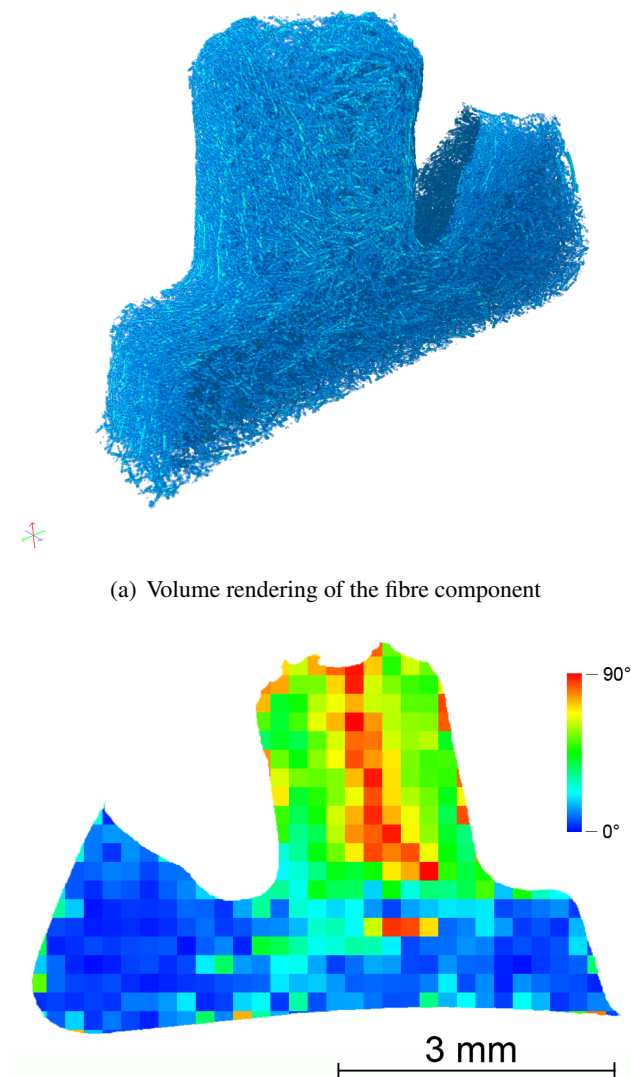
Of course, the two matrices given above are just two examples for the results which are available all throughout the dataset. In order to further visualize the local differences in the specimen's fibre system, we can compare these local orientation tensors to the global tensor in Eq. (12). We do that by classifying the entire volume into local areas which are aligned with the global fibre orientation tensor, and areas which are not – a process which can be thought of as an image segmentation algorithm. Using exactly this property, the layers depicted in Fig. 7 have been segmented. As a result, we find that the sample is actually composed of five layers parallel to the  $yz$ -plane with differently oriented carbon fibres: The layers contain fibres which are rotated roughly  $90^\circ$  with respect to the fibres in each neighbouring layer.

As a last application example, Fig. 8a shows the volume rendering of the CT reconstruction of a GFRP part from the automobile industry. It was imaged with a pixel size of  $6.7\mu\text{m}$  and is approximately  $6\text{mm}$  wide. The local fibre orientation analysis yields for the whole part

$$A^{(2)} = \begin{pmatrix} 0.270 & -0.016 & 0.027 \\ -0.016 & 0.286 & 0.002 \\ -0.027 & 0.002 & 0.444 \end{pmatrix}. \quad (13)$$

indicating a strong preference for the  $z$ -direction. However, in the most curved and thin areas, a significant deviation from this direction can be observed, see Fig. 8b.

The three application examples that have been presented here demonstrate the practical applicability of the methods described in this contribution. They show that fiber orientation tensors can be useful as a tool for very detailed, local analyses when inspecting them individually, as a qualitative tool for visualizing inhomogeneities such as layers, and as a quantitative tool when deriving specific quantities such as angular deviations.



(a) Volume rendering of the fibre component

(b) 2D slice through colour coded deviation from the main fibre direction

Fig. 8. Part made from glass fibre reinforced polymer. Volume rendering of the reconstructed CT image and 2D slice through 3D map of the deviation from the main fibre direction  $(-0.152, -0.026, -0.988)$ . Local orientation tensors are estimated in cubic subvolumes of edge length  $200\ \mu\text{m}$ .

## DISCUSSION

We have shown how the volume-weighted direction distribution computed from an image relates to the fibre direction distribution of a random fibre process. This relationship yields estimators not only for a discretised version of this spherical distribution, but also for its moments, the so-called orientation

tensors. Furthermore, four numerical schemes for implementing these estimators have been described. All of these schemes have the advantage of requiring only linear time in the number of pixels of a discrete image. The method based on the Hessian matrix is quite fast, accurate and robust. It is therefore recommended to compute volume-weighted direction distributions.

The limits of the proposed method follow mainly from the constraining assumption that we have placed on the dilated fibre process  $\Xi$ : Fibres must be solid, that is neither hollow nor featuring cavities. Fibre cross-sections have to be circular and of constant diameter. While the latter could be overcome by applying the local estimation method for different thicknesses and finally choosing the “strongest” local fibre direction, only the former is essential for all four considered methods. This assumption will however not be fulfilled for images of some natural materials such as cellulose fibres, for instance.

Therefore, the image analysis tools proposed in the present paper are particularly well suited for the analysis of glass or carbon fibre reinforced materials. This follows not only from their geometric properties. It also follows from the fact that orientation tensors, which can be directly computed using the tools described herewith, are important for the prediction of macroscopic mechanical properties of such composites.

The comparison clearly favours the two approaches based on partial derivatives while the method based on anisotropic Gaussian filters suffers from the need to sample the unit sphere. It does however have its merits for 2D applications, see Schladitz *et al.* (2016). There, the directional space corresponds to the unit circle, which is easy to sample uniformly and runtime limitations are much less of an issue.

All four methods were applied here “as is”, that means as described in the respective references. A hybrid method, combining, *e.g.*, the anisotropic Gaussian filters with the correction approach used for the main axis of inertia and the spatial smoothing step in the derivation of the structure tensor, could further increase efficiency and robustness.

One of the key assumptions in this presentation is the constant fibre radius for all fibres. Note that the axis of least inertia method does not require this. Moreover, for the partial grey value derivative based methods, it can be relaxed by varying the  $\sigma$  of the Gaussian in the smoothing step.

## ACKNOWLEDGMENTS

This work was supported in part by the German Federal Ministry of Education and Research through project 05M2013 (AniS), by the Center for Mathematical and Computational Modelling (CM)<sup>2</sup> and the Deutsche Forschungsgemeinschaft within the RTG 1932 “Stochastic Models for Innovations in the Engineering Sciences”.

## REFERENCES

- Advani S, Tucker C (1987). The use of tensors to describe and predict fibre orientation in short fiber composites. *J Rheol* 31:751–84.
- Altendorf H, Decencière E, Jeulin D, Peixoto P, Deniset-Besseau A, Angelini E et al (2012). Imaging and 3d morphological analysis of collagen fibrils. *J Microsc* 247:161–75.
- Altendorf H, Jeulin D (2009). 3d directional mathematical morphology for analysis of fiber orientations. *Image Anal Stereol* 28:143–53.
- Altendorf H, Jeulin D (2011). Random-walk-based stochastic modeling of three-dimensional fiber systems. *Phys Rev E* 83:041804.
- Bunge H (1993). On-line determination of texture-dependent materials properties. *J Nondestruct Eval* 12:3–11.
- Clarke A, Archenhold G, Davidson N (1995). A novel technique for determining the 3D spatial distribution of glass fibres in polymer composites. *Comp Sci Technol* 55:75–91.
- Eberhardt C, Clarke A (2001). Fibre-orientation measurements in short-glass-fibre composites. Part I: automated, high-angular-resolution measurement by confocal microscopy. *Comp Sci Technol* 61:1389–400.
- Eberly D, Gardner R, Morse B, Pizer S, Scharlach C (1994). Ridges for image analysis. *J Math Imaging Vis* 4:353–73.
- Fisher N, Lewis T, Embleton B (1987). *Statistical analysis of spherical data*. Cambridge, UK: Cambridge University Press.
- Fliege J, Maier U (1999). The distribution of points on the sphere and corresponding cubature formulae. *IMA J Numer Anal* 19:317–34.
- Frangi A, Niessen W, Vincken K, Viergever M (1998). Multiscale vessel enhancement filtering. In: *Proc Medical ICCA Intervention*. Lect Not Comput Sci 1496:130–7.
- Hu MK (1962). Visual pattern recognition by moment invariants. *IEEE T Inf Theory* 8:179–87.
- Kiderlen M, Pfrang A (2005). Algorithms to estimate the rose of directions of a spatial fibre system. *J Microsc* 219:50–60.
- Krause M, Hausherr J, Burgeth B, Herrmann C, Krenkel W (2010). Determination of the fibre orientation in composites using the structure tensor and local X-ray transform. *J Mater Sci* 45:888–96.
- Lampert C, Wirjadi O (2006). An optimal non-orthogonal separation of the anisotropic Gaussian convolution filter. *IEEE T Image Process* 15:3501–13.
- Lee J, Chung M, Alexander A (2006). Evaluation of anisotropic filters for diffusion tensor imaging. In: *Proc 3rd IEEE Int Symp Biomed Imaging*. April 6-9, Arlington, VA, USA. 77-8.
- Lee Y, Lee S, Youn J, Chung K, Kang T (2002). Characterization of fiber orientation in short fiber reinforced composites with an image processing technique. *Mater Res Innov* 6:65–72.
- Lindeberg T (1994). Scale-space theory: a basic tool for analyzing structures at different scales. *J Appl Stat* 21:224–70.
- Mecke J, Nagel W (1980). Stationäre räumliche Faserprozesse und ihre Schnitzzahlrosen. *Elektron Informationsverarb Kyb* 16:475–83.
- Nagel W (1983). Dünne Schnitte von stationären räumlichen Faserprozessen. *Math Operationsforsch Stat Ser Stat* 14:569–76.
- Ohser J, Schladitz K (2009). *3D images of materials structures: processing and analysis*. Weinheim: Wiley VCH.
- Ohser J, Steinbach B, Lang C (1998). Efficient texture analysis of binary images. *J Microsc* 192:20–8.
- Prokop RJ, Reeves AP (1992). A survey of moment-based techniques for unoccluded object representation and recognition. *CVGIP Graph Models Image Process* 54:438–60.
- Riplinger M, Spiess M (2012). Asymptotic properties of the approximate inverse estimator for directional distributions. *Adv Appl Probab* 44:954–76.
- Robb K, Wirjadi O, Schladitz K (2007). Fiber orientation estimation from 3D image data: Practical algorithms, visualization, and interpretation. In: *Proc Int Conf Hybrid Intelligent Systems*. Sept 17-19, Kaiserslautern, Germany. 320–5.
- Rosenfeld A, Pfaltz JL (1966). Sequential operations in digital picture processing. *J ACM* 13:471–94.
- Sandau K, Ohser J (2007). The chord length transform and the segmentation of crossing fibres. *J Microsc* 226:43–53.
- Schlادitz K, Büter A, Godehardt M, Wirjadi O, Fleckenstein J, Gerster T et al. (2016). Non-destructive characterization of fiber orientation in reinforced SMC

- as input for simulation based design. *Compos Struct* To appear.
- Tan J, Elliot J, Clyne T (2006). Analysis of tomography images of bonded fibre networks to measure distributions. *Adv Eng Mater* 8:495–500.
- Tankyevych O, Talbot H, Dokladal P, Passat N (2009). Direction-adaptive grey-level morphology. Application to 3d vascular brain imaging. In: *Proc. 16th IEEE Int Conf Image Proc (ICIP)*. November 7-10, Cairo, Egypt 2261–4.
- Weickert J (1999). Coherence-enhancing diffusion filtering. *Int Comp Vis* 31:111–27.
- Wirjadi O (2009). Models and algorithms for image-based analysis of microstructures. PhD thesis, Technische Universität Kaiserslautern.
- Wirjadi O, Schladitz K, Rack A, Breuel T (2009). Applications of anisotropic image filters for computing 2d and 3d-fiber orientations. In: *Proc 10th Europ Congr Stereol Image Anal*. June 22-26, Milano, Italy
- Yang H, Lindquist B (2000). Three-dimensional image analysis of fibrous materials. In: *Applications of Digital Image Processing XXIII*. July 30, San Diego, USA. *Proc SPIE* 4115:275.
- Young I, van Vliet L (1995). Recursive implementation of the Gaussian filter. *Signal Process* 44:139–51.
- Zhu YT, Blumenthal WR, Lowe TC (1997). Determination of non-symmetric 3-d fiber-orientation distribution and average fiber length in short-fiber composites. *J Compos Mater* 31:1287–301.